Online Thévenin Equivalent Determination Considering System Side Changes and Measurement Errors

Abdelkader, S. M., & Morrow, D. J. (2015). Online Thévenin Equivalent Determination Considering System Side Changes and Measurement Errors. IEEE Transactions on Power Systems, 30(5), 2716-2725. DOI: 10.1109/TPWRS.2014.2365114

Published in:
IEEE Transactions on Power Systems

Document Version:
Publisher's PDF, also known as Version of record

Queen's University Belfast - Research Portal:
Link to publication record in Queen's University Belfast Research Portal

Online Thévenin Equivalent Determination Considering System Side Changes and Measurement Errors

Sobhy M. Abdelkader, *Senior Member, IEEE*, and D John Morrow, *Member, IEEE*

***Abstract*—This paper presents a new method for online determination of the Thèvenin equivalent parameters of a power system at a given node using the local PMU measurements at that node. The method takes into account the measurement errors and the changes in the system side. An analysis of the effects of changes in system side is carried out on a simple two-bus system to gain an insight of the effect of system side changes on the estimated Thévenin equivalent parameters. The proposed method uses voltage and current magnitudes as well as active and reactive powers; thus avoiding the effect of phase angle drift of the PMU and the need to synchronize measurements at different instances to the same reference. Applying the method to the IEEE 30-bus test system has shown its ability to correctly determine the Thévenin equivalent even in the presence of measurement errors and/or system side changes.**

***Index Terms*—Phasor measurement, power system, Thévenin equivalent.**

I. Introduction

THÉVENIN equivalent (TE) at a node offers a simple, yet accurate, abstraction of the system as seen from that node. This enables a wide variety of monitoring, assessment, and control techniques to be implemented locally without the need for the unwanted, and/or unavailable, details of the system. This fact has been the motivation for continuous interest in the TE for several different purposes and has resulted in many interesting methods and techniques for TE determination.

TE has been, and is being, used for a wide variety of applications including, but not limited to: short circuit current calculation in both distribution [1], [2] and transmission systems [3]; fault location [4], [5]; parameter identification for instability detection [6] and for electromagnetic transient studies [7]; harmonic detection and analysis in distribution systems [8], [9]; under voltage load shedding [10]; online estimation of maximum power transfer limits [11]; and voltage stability monitoring [12]–[20].

Methods for determining the TE parameters, depending on the application, have many different bases. The TE in an unbalanced three-phase system is obtained by measurements of the root mean square (RMS) values of terminal voltages and currents [20], inverting the 3-phase $\mathbf{Y_{bus}}$[3], or determining the multiphase $\mathbf{Z_{th}}$ matrix either by load insertion [2] or current injection [1] at each phase one at a time. For harmonic detection, $\mathbf{Z_{th}}$ is determined and compared with the critical impedance [8], while in [9], the harmonic source is characterized by a Norton equivalent determined by making a change in the system side, changing the transformer tap. Least squares estimation [10], [15] and optimization [22] techniques were also used to determine the TE.

Using $\mathrm{Z_{th}}$ to assess local voltage stability is very common and different methods for determining $\mathrm{Z_{th}}$ for this purpose were introduced. Tallegen's Theorem was utilized in [12], network decoupling transform [13], local PMU measurement based TE in [14], [16], [17], $\mathrm{Z_{bus}}$ in [18], and multiple power flow in [19] and [20].

The availability of PMU measurements has opened the door to different possibilities of online determination of the TE and to enhance the system monitoring and control functions using the TE. In [23], a method for determining TE utilizing three PMU measurements, where two circular loci in the Z-plane were defined each using two measurements. The intersection of the two loci determines Z_{TH} and hence E_{TH} is determined using the voltage equation for any of the measurements. This method was successfully utilized in [4] to develop an adaptive fault location algorithm for power systems and in [5] to develop a fully adaptive algorithm for series compensated lines.

In a previous work [24], [25], the authors developed a method where three PMU measurements were first synchronized to the same reference and then used to determine the TE parameters. Application of this method to real measurements has demonstrated good accuracy in steady-state system conditions. However, this was not the case when applied to data recorded during arduous weather conditions causing multiple transient and permanent loss of generation and transmission capacity. Also, variations taking place in the system side due to high penetration of variable wind generation now typically experiences on the island of Ireland greatly affect the accuracy of this method. This is because the method of [24] and [25]

Manuscript received May 18, 2014; revised August 01, 2014 and September 18, 2014; accepted October 21, 2014. Date of publication November 03, 2014; date of current version July 17, 2015. This work was supported by a Charles Parsons Energy Research Award, which is funded by the Science Foun- dation Ireland (SFI), award (06/CP/E002). Paper no. TPWRS-00628-2014.

S. M. Abdelkader is with the Electrical Engineering Department, Mansoura University, Mansoura, Egypt, and also with the School of Electronics, Electrical Engineering, and Computer Science, Queen's University Belfast, Belfast BT9 5AH, U.K. (e-mail: s.abdelkader@qub.ac.uk).

D J. Morrow is with the School of Electronics, Electrical Engineering, and Computer Science, Queen's University Belfast, Belfast BT9 5AH, U.K. (e-mail: dj.morrow@ee.qub.ac.uk).

Color versions of one or more of the figures in this paper are available online at http://ieeexplore.ieee.org.

Digital Object Identifier 10.1109/TPWRS.2014.2365114

requires that the system side remains unchanged during the three measurements interval for the synchronization process to be successful, which may not be the case during the aforementioned conditions. Therefore, the aim of this work is to develop a method that is tolerant of system variations during determination of the TE parameters.

This paper presents a new method for online determination of TE parameters that avoids the need to synchronize the measurements at different time instances and is able to deal with system side changes as well as the measurement errors. A number of measurements are used to determine straight-line loci for the relationship between r and x of Z_{TH} in the Z plane. Intersection points of these lines represent the possible values of Z_{TH}. The probability distribution of the estimated values of Z_{TH} is constructed and the value with the highest probability is taken as Z_{TH}.

II. Proposed Method

A. Background

According to Thévenin's theorem, any active network can be represented by an equivalent having a single voltage source connected to a single equivalent series impedance. It should be made clear that, when applied to a power system, the equivalent source voltage and impedance will change following any change in the network. However, in the short term, a few cycles, variations in a large system are not expected to cause significant variations in the estimated TE equivalent parameters. Measurements over this short period can be used to find an equivalent that can represent the system during that short period of time. On the other side, a load or even local generation at one node may experience much greater variation than the rest of the system, which has a greater inertia and more reserves and typically less load variation due to aggregation and diversity of a large number of loads scattered over a wider geographical area. It is a fact that changes on the load side will affect the system side; however even very large change in the load side will only slightly affect the system side. An analogy to this is a small vessel connected to a huge water reservoir; the change of water level in the vessel either when filling or drainage will not cause noticeable effect on the water level in the reservoir. It is possible however to determine the water level in the reservoir by the rate of water flow into the vessel.

Determination of the Thèvenin equivalent for a system at a node using measurement is thus based on the assumption that the part of the system on one side of the node is stable or its variation is slow enough not to affect the measurements used for one calculation step; this side is termed "system side" in Fig. 1. The part on the other side of the measurement node is assumed to be changing and it is termed "load side" in Fig. 1. It can be proven that two measurements of voltage/current pairs at the point of interest are enough to determine a Thèvenin equivalent for the stable side, the system side. In the analysis below, the subscript "S" defines system side parameters where as "L" will subscript load side parameters.

Assuming that the equivalent source voltage and impedance of the system side are E_S and Z_S, respectively, and those of the load side are E_L and Z_L, the current and voltage measured at the point of common coupling can be determined in terms of the equivalent parameters of the two sides as follows:

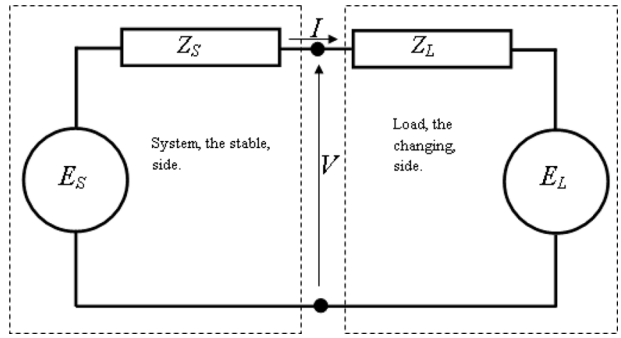

Fig. 1. System equivalents on both sides of a measurement point.

$$I_1 = \frac{E_S - E_L}{Z_S + Z_L} \tag{1}$$

$$V_1 = \frac{E_S Z_L + E_L Z_S}{Z_S + Z_L}. \tag{2}$$

However, in modern power system with large penetration of variable non-dispatchable energy generators, it cannot be guaranteed that the system side will remain unchanged for any time interval no matter how small. How variation in the system side will affect the measurement-based TE parameter estimation is the main issue of the analysis in the following section.

B. Effect of System Side Changes and Measurement Errors

Now assuming that E_S, Z_S, E_L, and Z_L have experienced per unit changes of δ_{ES}, δ_{ZS}, δ_{EL}, and δ_{ZL}, respectively, the current and voltage at the measurement point will change to I_2 and V_2, where

$$I_2 = \frac{E_S(1+\delta_{ES}) - E_L(1+\delta_{EL})}{Z_S(1+\delta_{ZS}) + Z_L(1+\delta_{ZL})} \tag{3}$$

$$V_2 = \frac{\mathrm{E_S}(1+\delta_{\mathrm{ES}})\mathrm{Z_L}(1+\delta_{\mathrm{ZL}}) + \mathrm{E_L}(1+\delta_{\mathrm{EL}})\mathrm{Z_S}(1+\delta_{\mathrm{ZS}})}{\mathrm{Z_S}(1+\delta_{\mathrm{ZS}}) + \mathrm{Z_L}(1+\delta_{\mathrm{ZL}}).} \tag{4}$$

The two measurement pairs (V_1, I_1) and (V_2, I_2) can now be used to determine a Thèvenin equivalent for the system side based on the assumed current flow direction shown in Fig. 1. The Thèvenin equivalent parameters can be determined as shown by (5) and (6):

$$Z_{TH} = \frac{V_1 - V_2}{I_2 - I_1} \tag{5}$$

$$E_{TH} = \frac{V_1 I_2 - V_2 I_1}{I_2 - I_1.} \tag{6}$$

Substituting for V_1, I_1, V_2, and I_2 from (1)–(4) into (5), Z_{TH} can be proven to be (7), shown at the bottom of the next page.

Examining the last term in the numerator of (7), it includes a combination of the products of per unit variations of both sides, $\delta_{ES}\delta_{ZL}$ and $\delta_{EL}\delta_{ZS}$, which will be always zero under the assumption that change takes place in one side only. Hence these

terms can be omitted and (7) is reduced to (8) at the bottom of the page.

Similarly, using the values of V_1, I_1, V_2, and I_2 in (6), E_{TH} can be found to be (9) at the bottom of the page.

Again, with the assumption that only one side changes, the third term in the numerator of (9) can be omitted and (9) reduces to (10) at the bottom of the page.

If the system side remains unchanged, both δ_{ES} and δ_{ZA} will be zero. When zero is substituted for δ_{ES} and δ_{ZS} in (8) and (10), Z_{TH} and E_{TH} will be as follows:

$$Z_{TH} = \frac{(-\delta_{ZL})Z_S Z_L(E_S - E_L) - (\delta_{EL} Z_S E_L)(Z_S + Z_L)}{-(\delta_{ZL} Z_L)(E_S - E_L) + (-\delta_{EL} E_L)(Z_S + Z_L)} = Z_S \tag{11}$$

$$E_{TH} = \frac{(-\delta_{EL})E_S E_L(Z_S + Z_L) - (+\delta_{ZL} Z_L E_S)(E_S - E_L)}{(-\delta_{EL} E_L)(Z_S + Z_L) - (\delta_{ZL} Z_L)(E_S - E_L)} = E_S. \tag{12}$$

If the system side is the changing side while the load side remains unchanged, both δ_{EL} and δ_{ZL} are set to zero in (8) and (10), yielding the values of Z_{TH} and E_{TH} as follows:

$$Z_{TH} = \frac{(\delta_{ZS})Z_S Z_L(E_S - E_L) - (\delta_{ES} Z_L E_S)(Z_S + Z_L)}{-(\delta_{ZS} Z_S)(E_S - E_L) + (\delta_{ES} E_S)(Z_S + Z_L)} = -Z_L \tag{13}$$

$$E_{TH} = \frac{(\delta_{ES})E_S E_L(Z_S + Z_L) - (\delta_{ZS} Z_S E_L)(E_S - E_L)}{(\delta_{ES} E_S)(Z_S + Z_L) - (\delta_{ZS} Z_S)(E_S - E_L)} = E_L. \tag{14}$$

It is now clear from the way the TE is calculated that the equivalent for the stable side is always determined, irrespective if this is the system or the load side. The sign of Z_{TH} is the indicator to which side the calculated equivalent belongs. It is also clear that one side has to remain unchanged so that its TE can be calculated. However, it happens sometimes that both sides experience changes in the time between measurement instances.

To study the effect of simultaneous variations in both sides on the determined TE, E_S, Z_S, E_L, and Z_L of Fig. 1 are assumed to be 1.01, 0.1, 1, and 2.0, respectively, all in per unit, for simulating the first measurement pair (V_1, I_1). For simulating the second measurement, variations are introduced in both sides. Variations ranging from -1% to $+1\%$ are introduced in the system side parameters, whereas -10% to $+10\%$ variations were introduced in the load side parameters in 21 steps for each. V_2 and I_2 are determined for each of the possible combinations of the changed parameters. Each of the determined (V_2, I_2) pairs are used along with (V_1, I_1) to determine a TE for each case of parameter changes.

Variation of Z_{TH} with variations in Z_S and Z_L is shown in Fig. 2(a), which reveals that the calculated Z_{TH} is almost equal to Z_S except at zero variation in Z_L where Z_{TH} becomes equal to $-Z_L(-2\text{ pu})$. The value of Z_{TH} is more affected when the variation in Z_L is very small and of the same order of variations in Z_S; this is shown in Fig. 2(b), which is similar to Fig. 2(a) but excluding the case of unchanged Z_L to make variations in Z_{TH} of the system side more clear. It may be observed from the figure

$$Z_{TH} = \frac{(\delta_{ZS} - \delta_{ZL})Z_S Z_L(E_S - E_L) - (\delta_{ES} Z_L E_S + \delta_{EL} Z_S E_L)(Z_S + Z_L) - (\delta_{ES}\delta_{ZL} E_S + \delta_{EL}\delta_{ZS} E_L)(Z_S + Z_L)}{-(\delta_{ZS} Z_S + \delta_{ZL} Z_L)(E_S - E_L) + (\delta_{ES} E_S - \delta_{EL} E_L)(Z_S + Z_L)} \tag{7}$$

$$Z_{TH} = \frac{(\delta_{ZS} - \delta_{ZL})Z_S Z_L(E_S - E_L) - (\delta_{ES} Z_L E_S + \delta_{EL} Z_S E_L)(Z_S + Z_L)}{-(\delta_{ZS} Z_S + \delta_{ZL} Z_L)(E_S - E_L) + (\delta_{ES} E_S - \delta_{EL} E_L)(Z_S + Z_L)} \tag{8}$$

$$E_{TH} = \frac{\begin{array}{c}(\delta_{ES} - \delta_{EL})E_S E_L(Z_S + Z_L) \\ -(\delta_{ZS} Z_S E_L + \delta_{ZL} Z_L E_S)(E_S - E_L) \\ -(\delta_{EL}\delta_{ZS} E_L Z_S + \delta_{ES}\delta_{ZL} E_S Z_L)(E_S - E_L)\end{array}}{-(\delta_{ZS} Z_S + \delta_{ZL} Z_L)(E_S - E_L) + (\delta_{ES} E_S - \delta_{EL} E_L)(Z_S + Z_L)} \tag{9}$$

$$E_{TH} = \frac{(\delta_{ES} - \delta_{EL})E_S E_L(Z_S + Z_L) - (\delta_{ZS} Z_S E_L + \delta_{ZL} Z_L E_S)(E_S - E_L)}{(\delta_{ES} E_S - \delta_{EL} E_L)(Z_S + Z_L) - (\delta_{ZS} Z_S + \delta_{ZL} Z_L)(E_S - E_L)} \tag{10}$$

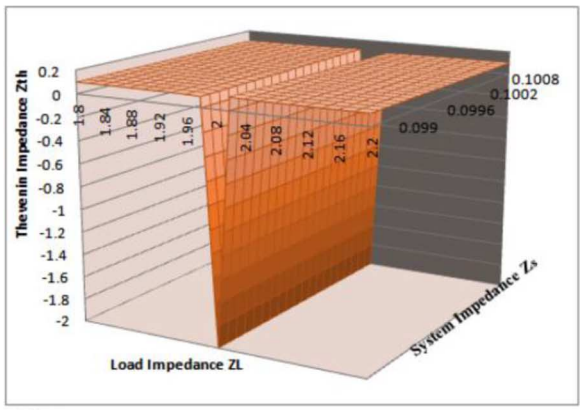

a.

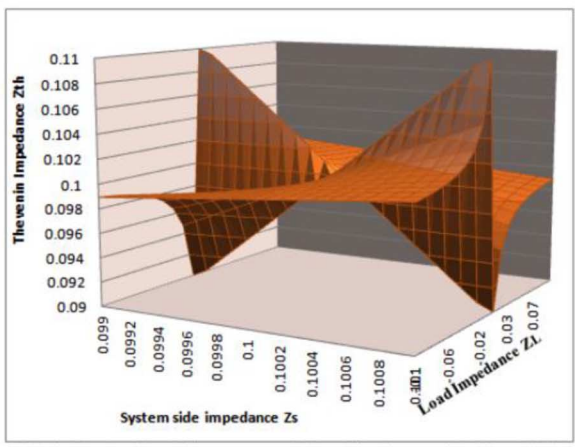

b.

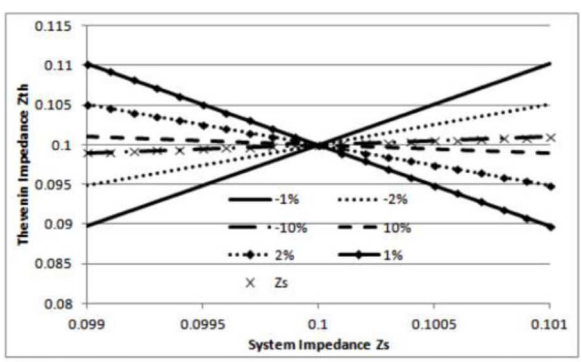

c.

Fig. 2. Effect of Z_S and Z_L variations on Z_{TH}. (a) Variation of the estimated Z_{th} with variation in Z_S and Z_L. (b) Variation in Z_{th} of the system side with changes in Z_L and Z_S. (c) Z_{TH} variation with changes in Z_S for different changes in Z_L.

that the estimated Z_{TH} is almost equal to Z_S as it is the side of smaller variation. However when the variation in Z_L is very small, the error in Z_{TH} is of the order of $\pm 10\%$. This is shown more clearly in Fig. 2(c) where variations of Z_{TH} at specific values of variations in Z_L are drawn against variations in Z_S; the correct value of Z_{TH} should be equal to Z_S, which is drawn on the figure by the "$\times$" marker. It is clear from that figure that if Z_S changed the error in Z_{TH}, it is smaller when larger variation takes place in Z_L. Of course the error in Z_{TH} will depend on the ratio of the system side to the load side short-circuit ratio. In the present case, the system short circuit level is taken 20 times the

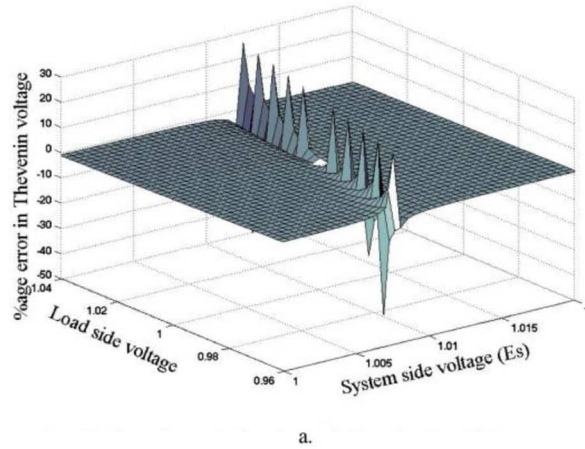

a.

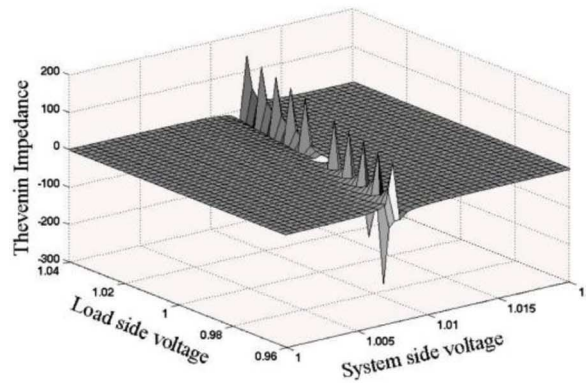

b.

Fig. 3. Effect of E_S and E_L variations on Z_{TH}. (a) Error in the estimated E_{th} with variations in E_S and E_L. (b) Variation of the estimated Z_{th} with variations in E_S and E_L.

load level, which is quite low for a transmission system but was deliberately chosen just to highlight the effect of system side change. A stronger system with larger short circuit/load ratio, i.e., higher Z_L/Z_S, will have smaller errors in Z_{TH} estimation.

It should be noted that changes in system impedance are less likely to take place. Typically, unless a switching operation has taken place, the system impedance remains relatively constant. The impedance measured at a given node will, of course, be affected by changing loads at other system nodes. However, the speed and order of change are not significant in the context of TE calculation. Changes in generators' voltages, when they occur, are faster and affect the system side voltage, equivalent E_S of Fig. 1.

Fig. 3 depicts the effects of simultaneous variations in E_S and E_L on the determined E_{th} and Z_{TH}. Fig. 3(a) shows the percentage error in E_{th} against the variations in both E_S and E_L. It can be observed that the error is very small, or almost zero, everywhere except when the change in E_L is comparable to the change in E_S. The error in E_{TH} due to variations in E_S and E_L lies within the -40% to 30% range. These figures are specific for the simple system of Fig. 1 and the aforementioned values of its elements; nonetheless, it clarifies some issues, which helps to explain and diagnose the reasons behind the occasional "odd" value of TE parameters estimated from real system measurements. Fig. 3(b) shows the variation of Z_{TH} with E_S and E_L.

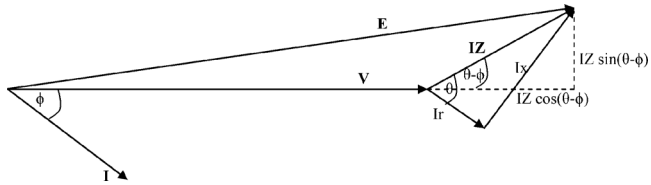

Fig. 4. Phasor diagram of the measurement node.

It will be noticed that the error in the estimated $Z_{\rm TH}$ follows almost the same pattern as that of the estimated E_{TH}; however, the magnitude of the error in $Z_{\rm TH}$ is much larger (20 000% for some cases when the variation in E_S and E_L are of the same order).

The above analysis makes some points clear regarding the estimation of TE as follows: 1) the estimated TE will be the equivalent of the side with less variation, 2) sign of the determined Z_{TH} indicates to which side the estimated TE belongs, 3) variation of either E_S or Z_S causes error in both of the estimated Z_{TH} and E_{TH}, and 4) the error in the estimated TE parameters becomes very large when the change in the system side is of the same order of the change in load side.

C. Method for TE Determination

This section details the proposed method for determining the TE and the procedural steps for its implementation. To simplify the equations Z, E, r, and x, refer to the TE parameters without the need to the subscript "$_{\rm TH}$".

Consider the phasor diagram of Fig. 4 representing the relationship between the measured quantities V and I and the Thèvenin equivalent parameters E and Z.

From the geometry of the figure, it is clear that

$$E^2 = (V + IZ\cos(\theta-\phi))^2 + (IZ\sin(\theta-\phi))^2 \tag{15}$$

or alternatively

$$E^2 = V^2 + I^2Z^2 + 2Pr + 2Qx. \tag{16}$$

P and Q are the active power and reactive power, respectively. For three different measurements

$$E^2 = V_1^2 + I_1^2Z^2 + 2P_1r + 2Q_1x \tag{17}$$
$$E^2 = V_2^2 + I_2^2Z^2 + 2P_2r + 2Q_2x \tag{18}$$
$$E^2 = V_3^2 + I_3^2Z^2 + 2P_3r + 2Q_3x. \tag{19}$$

Subtracting (18) from (17), and (19) from (18), we get

$$V_1^2 - V_2^2 + (I_1^2 - I_2^2)Z^2 + 2(P_1 - P_2)r + 2(Q_1 - Q_2)x = 0 \tag{20}$$
$$V_2^2 - V_3^2 + (I_2^2 - I_3^2)Z^2 + 2(P_2 - P_3)r + 2(Q_2 - Q_3)x = 0. \tag{21}$$

Eliminating Z^2 from (20) and (21) yields

$$\begin{aligned}&(V_1^2 - V_2^2)(I_2^2 - I_3^2) - (V_2^2 - V_3^2)(I_1^2 - I_2^2)\\ &\quad + 2((P_1 - P_2)(I_2^2 - I_3^2) - (P_2 - P_3)(I_1^2 - I_2^2))r\\ &\quad + 2((Q_1 - Q_2)(I_2^2 - I_3^2) - (Q_2 - Q_3)(I_1^2 - I_2^2))x = 0.\end{aligned} \tag{22}$$

Arranging the coefficients of r, x, and the first two terms of (22), it can be written as follows:

$$2\Delta Pr + 2\Delta Qx + \Delta V^2 = 0 \tag{23}$$

where

$$\Delta P = \det\begin{bmatrix}1 & 1 & 1\\ P_1 & P_2 & P_3\\ I_1^2 & I_2^2 & I_3^2\end{bmatrix},$$
$$\Delta Q = \det\begin{bmatrix}1 & 1 & 1\\ Q_1 & Q_2 & Q_3\\ I_1^2 & I_2^2 & I_3^2\end{bmatrix}, \text{ and}$$
$$\Delta V^2 = \det\begin{bmatrix}1 & 1 & 1\\ V_1^2 & V_2^2 & V_3^2\\ I_1^2 & I_2^2 & I_3^2\end{bmatrix}. \tag{24}$$

It may have become clear now that a group of three different measurements can produce a line representing the relationship between the Thèvenin impedance parameters r and x. As shown by (23) and (24), constructing (23) is simple and can be done in a structured and systematic way. Also, a very important feature of (23) is that there is no need for synchronizing the measurements to the same reference as all the quantities used are scalar quantities.

Equation (23) can be solved along with either (20) or (21) to obtain the values of r and x. However, in the case of a change in the system side of a relative magnitude comparable to the change in the load side, there may be no solution. Also, when two consecutive measurements have equal or very close values, the coefficients of (23) will be zeros and no solution can be obtained.

The widely accepted practice to account for measurement errors, and the small variations in the system side, is to use redundant measurements. Adding more measurements produces new linear relationships between r and x. For example, adding a 4th point to those of (17)–(18), four different straight-line equations like (23) can be obtained. Four different lines will have up to 6 intersection points; each of these points locates a value of Z_{TH} in the impedance plane. In the ideal case, where the system is unchanging and there are no measurement errors, all of these points will coalesce in one point giving one value for Z_{TH}. Depending on the magnitudes of system side change and/or measurement errors, some of the points will deviate from the correct location. It is also to be noted that if both the system and load sides are unchanged so that two the measurements are the same, some of the lines will be coincident to each other, giving no indication about the location of Z_{TH}. Therefore, it would be better to use more measurement points in each determination of Z_{TH}.

However, the number of measurements used per calculation step has to be properly chosen. Large number of measurements will of course help providing the required redundancy, but at the same time may bring measurement points for a totally different system state into the calculation cycle. This may cause a deviation from the correct TE value due averaging effect and/or masking short-term events such as considerable transient variations in system impedance. N measurements will produce C_3^N possible combinations of different threes out of N straight lines as defined by (23). The maximum number, N_Z, of intersection

points, values of Z_{TH}, of these lines is the possible combinations of two lines out of the total number of lines. It can be proven that (as shown in the Appendix)

$$N_Z = \frac{N(N-1)(N-2)(N(N-1)(N-2)-6)}{72}. \quad (25)$$

For $N = 4$, then N_Z is 6; if $N = 5$, then N_Z will be 45; whereas and if $N = 6$, then N_Z is as high as 190. Higher values of N will make N_Z get very high ($N = 7 \rightarrow N_Z = 1415$) and the measurements will span a longer time interval where changes are more likely to take place in the system side. Through different trials with different numbers of measurements, five measurements have been found to achieve the suitable balance between the above-mentioned factors (accounting for measurement errors and system changes and at the same time avoiding relatively large changes in the system side). Also, the number of impedance values, N_Z, is 45, which is sufficient to be represented by a normal distribution to estimate the value of Z_{TH} to an adequate confidence level.

D. Calculation Procedure

1) For each of the most recent five $(V,\ I)$ PMU measurement pairs, determine P, Q using the voltage and current phasors.
2) Construct the ten possible triples $(\Delta\mathrm{P},\ \Delta\mathrm{Q},\ \Delta\mathrm{V}^2)$ as defined by (24); each of these triples represents the coefficients of a straight line as defined in (23).
3) For each pair $\{(\Delta\mathrm{P},\ \Delta\mathrm{Q},\ \Delta\mathrm{V}^2)_\mathrm{i}, (\Delta\mathrm{P},\ \Delta\mathrm{Q},\ \Delta\mathrm{V}^2)_\mathrm{j}, i \neq j\}$ of the ten triples of step 2, determine the TE parameters r and x, the intersection of the two lines defined by these two triples as follows:

$$r = \frac{\Delta Q_i.\Delta V_j^2 - \Delta Q_j.\Delta V_i^2}{2(\Delta P_i \Delta Q_j - \Delta P_i \Delta Q_j)} \quad (26)$$

$$x = \frac{\Delta P_j.\Delta V_i^2 - \Delta P_i.\Delta V_j^2}{2(\Delta P_i \Delta Q_j - \Delta P_j \Delta Q_i)}. \quad (27)$$

4) The frequency distributions of the estimated r and x values are then determined and the values of r, x that have the largest frequencies are taken the TEs. It is also possible to determine the probability distributions of r and x values and determine their values range to any desired confidence level.
5) Having r and x, E can be determined using (16).

The following section presents the application of the proposed method with illustration of the calculation steps.

III. Application Results and Discussion

To test the accuracy of the proposed method and its resilience to system variations, it was necessary to have measurements where accurately known system variations are taking place. The same is true for testing the ability of the proposed method to tolerate measurement error; measurements incorporating preknown errors are necessary. However, it is almost impossible to find data sets that meet these requirements. Therefore, the use of a test system was essential to generate data sets for different known test conditions. The IEEE 30-bus system [26] was used for this purpose and different test cases were simulated to emulate PMU measurements, which are used to test the proposed method.

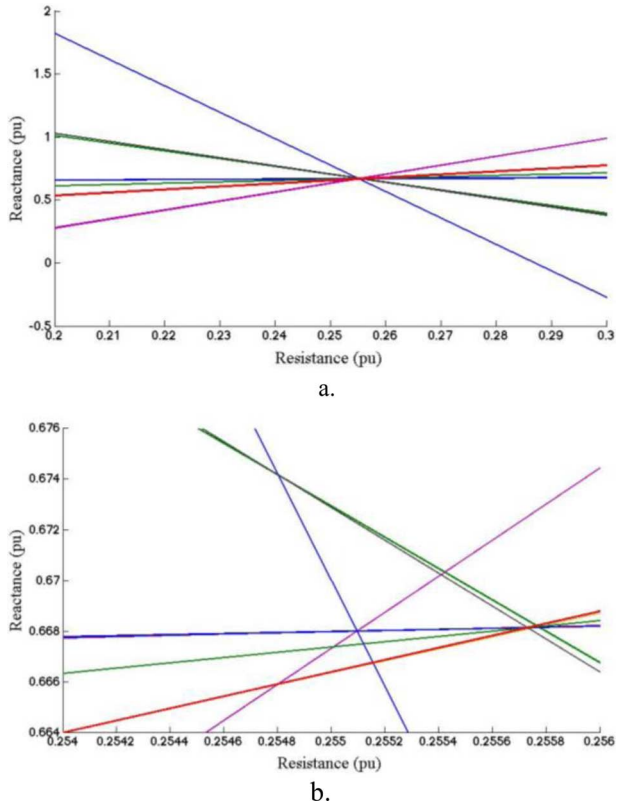

Fig. 5. Impedance loci and solutions in the Z-plane. (a) x/r relationship loci in Z-plane. (b) Z_{TH} solutions.

A. Test System Results

The first test was carried out with simulated measurements of the test system where everything was kept constant except the load at bus 30. The load at this bus was varied by the introduction of random variations of both the magnitude and angle of voltage and current at this node. Loads at all nodes were recorded and used as PMU measurements. To show how the proposed method works, details of one calculation step are presented in Fig. 5. The ten lines representing the relationships between r and x, for 5 measurements, are obtained using (9) and drawn in Fig. 5(a).

It is clear that some lines coincide and that all lines intersect at almost the same point. To have a clearer idea, the region of lines intersections is magnified and depicted in Fig. 5(b). It may be observed from this more detailed view that all lines do not intersect at exactly the same point, yielding different values of r and x. However, the ranges of r and x values are very narrow, (0.2548–0.2558) for r and (0.666–0.674) for x. These small variations in the values of TE parameters are due to constant P constant Q representation of loads, rather than constant impedances. Variations of voltages at load buses cause small variations in the equivalent load impedance at these buses. This is reflected in the estimated values of the TE parameters. However, as it is clear from Fig. 5(b), the range of these variations is very small (0.39% for r and 1.19% for x).

The frequency distributions of the calculated TE parameters for four different calculations steps are displayed in Fig. 6. It is clear that the range of estimated values of r and x is very narrow and hence the variance is very small. Thus, the mean

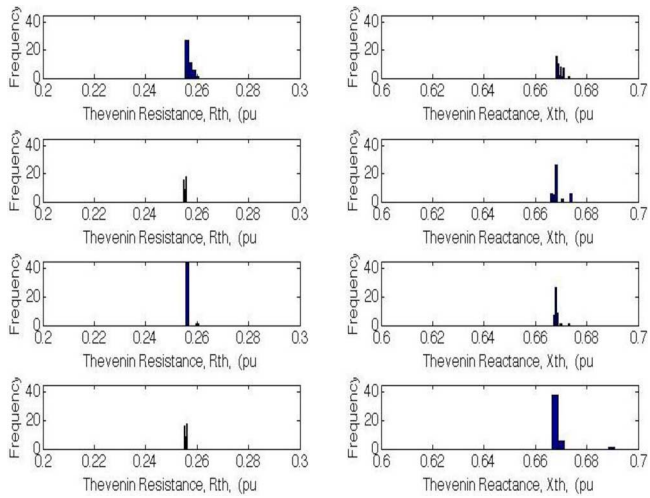

Fig. 6. Frequency distribution of r and x values.

TABLE I
MEAN AND STANDARD DEVIATION OF TE PARAMETERS

Mean(r)	σ_r	$\%\,\sigma_r$	*Mean(x)*	σ_x	$\%\sigma_x$
0.2550	0.0003	0.1088	0.6692	0.0006	0.0919
0.2553	0.0006	0.2209	0.6684	0.0009	0.1418
0.2554	0.0017	0.6535	0.6762	0.0019	0.2878
0.2559	0.0001	0.0496	0.6703	0.0006	0.0957
0.2556	0.0007	0.2778	0.6719	0.0052	0.7803
0.2556	0.0010	0.3869	0.6724	0.0069	1.0256
0.2544	0.0013	0.4956	0.6690	0.0012	0.1758
0.2551	0.0021	0.8342	0.6692	0.0009	0.1295
0.2564	0.0030	1.1714	0.6685	0.0024	0.3630
0.2554	0.0012	0.4765	0.6692	0.0009	0.1380
0.2556	0.0011	0.4374	0.6686	0.0024	0.3577
0.2559	0.0022	0.8581	0.6666	0.0085	1.2733
0.2563	0.0011	0.4248	0.6664	0.0048	0.7245
0.2550	0.0001	0.0339	0.6702	0.0002	0.0275
0.2528	0.0013	0.5013	0.6707	0.0035	0.5237
0.2551	0.0008	0.3157	0.6702	0.0021	0.3113

value and the value with the highest frequency will be of very similar value, and either can be considered as the estimated TE parameter. Table I lists the mean values, the standard deviation both absolute and percent of the mean values for r and x for the case of unchanged system side. It may be observed that the standard deviation of estimated r and x is very small, almost less than 1% of the mean. Thus, the estimated TE parameters are obtained with a very high accuracy. However, this is the case when the system side remains unchanged.

It is also necessary to evaluate if the same level of accuracy can be obtained in the TE values when there are changes on the system side. For this purpose, different system side changes were simulated including increasing loads on all system buses and switching operations. Loads at all buses are simultaneously scaled by factors of 1.1, 1.3, and 1.5. At each of these scale factors, load at bus 30, the load side, was changed; voltage and current at bus 30 were recorded to simulate PMU measurements. Fig. 7 shows the variations of the TE parameters r and x. The first part of this figure displays r and x for measurement points obtained by changing load at bus 30 while keeping loads at other buses constant at its standard case values.

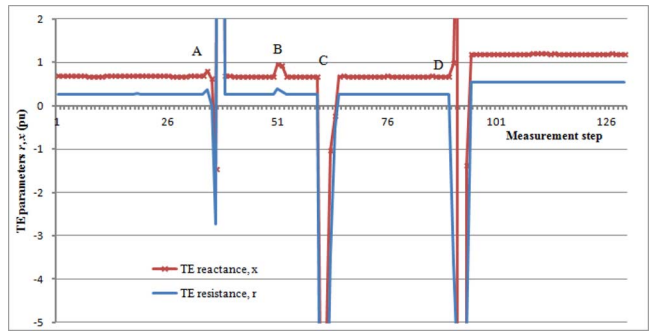

Fig. 7. TE parameters for system side variations of the test system.

TABLE II
VARIATIONS IN THE SYSTEM SIDE

Point	System Side Variations			Load side
	Load var.	*Generation*	*Switching*	
A	+10%	Rescheduled	--	variable
B	+20%	Const V,δ	--	variable
C	+20%	reshedueled	--	Fixed for 5 steps
D	0	Const V,δ	Line 27-30 out	variable

At point A, loads at all load buses were increased to 110% of the standard case while varying load at bus 30 at the same time. It can be observed that the values of the estimated TE parameters in such circumstances have experienced large variations for 4 calculation steps and then returned to their original values.

At point B, all loads were increased to 130% of their original values, but in this case, the magnitudes and angles of generators' voltages were kept constant. It will be noted that the variations in the estimated TE parameters are significantly lower than in the previous case. This indicates that variation of generators' voltages affects the estimated TE parameters more than system side load variations.

At point C, loads at all system buses were increased to 150%, but load at bus 30 was kept constant for 5 steps. The estimated TE equivalents in this case are found to be negative, pointing to the load side equivalent impedance.

At point D, line 27–30 was disconnected. After variations in the determined TE present for 5 steps, the TE parameters assume almost constant new values higher than those observed prior to disconnection of the line. Resistance and reactance have increased from (0.26, 0.67) before line tripping to (0.39, 1.2) after line tripping.

These variations in the system side are summarized in Table II. It is to be noted that the values of TE parameters calculated by the proposed method are similar to those determined by different methods reported in [19], [23], and [24]. For the methods of [23] and [24] to give the correct values of TE parameters, the system side has to remain unchanged during the period of the 3 measurements steps used for calculation, which cannot be guaranteed all the time. The phase angle drift caused by system frequency changes affects the TE parameters determined by the method of [24]; hence, it requires the synchronization of the measurements before using it. The proposed

TABLE III
MEAN AND STANDARD DEVIATION OF TE PARAMETERS DURING SYSTEM VARIATION

Point	*Mean(r)*	σ_r	*Mean(x)*	σ_x
A	0.362	0.261	0.800	0.113
	-0.015	0.725	0.616	0.431
	-2.737	5.589	-1.470	4.643
	25.161	57.052	21.909	47.821
B	0.263	0.002	0.674	0.002
	0.384	0.295	0.949	0.269
	0.335	0.441	0.931	0.310
	0.259	0.002	0.672	0.002
C	0.262	0.007	0.673	0.006
	-11.149	24.946	-7.575	19.044
	-9.090	25.616	-6.095	19.606
	-3.482	19.271	-1.034	15.471
	-0.513	1.305	-0.229	1.919
	0.256	0.006	0.668	0.006
D	0.260	0.000	0.672	0.000
	-3.640	2.406	0.982	3.869
	-5.847	0.980	5.176	2.732
	-5.934	1.154	1.538	2.766
	-5.274	3.575	-1.390	3.915
	0.540	0.003	1.190	0.000

method, on the other hand, is not affected by the phase angle drift and can tolerate system side changes.

Table III lists mean values and standard deviation of the TE parameters around the points of change. The standard deviations at these points are high, which is to be expected. However, the TE parameters return to their stable values as soon as the change comed to an end and the calculation window has passed over the measurements recorded during the period of change.

B. Application to Real System Measurements

PMU measurements are being collected for more than 4 years from different locations in Northern Ireland (NI) and being used for different purposes. Details of the Northern Ireland system can be found in [27]. PMU measurements are saved in files each contain 5-min measurements. The proposed method has been applied to the measurements recorded at the one node, the terminals of a wind farm in NI. Fig. 8 presents the values of TE parameters, r and x in (a) whereas E_{th} and the terminal voltage in (b), against time. The figure spans 10 min, which equates to 30 000 PMU records. These 10-min data were selected from measurements recorded during arduous weather conditions that was causing numerous transient and in fact resulted in permanent system faults resulting in loss of generation and transmission capacity. From the figure, it can be observed that between 23:14 and 23:21, the system impedance varies slightly around an almost constant average. Variations during this period are similar to those at point B of Fig. 6; therefore, we believe these variations are due to the continuous changes in the system side due to automatic generation control (AGC) actions. The two spikes in the TE parameters during this period are due to unsuccessful trials of reclosing the CB of a tripped circuit of a transmission

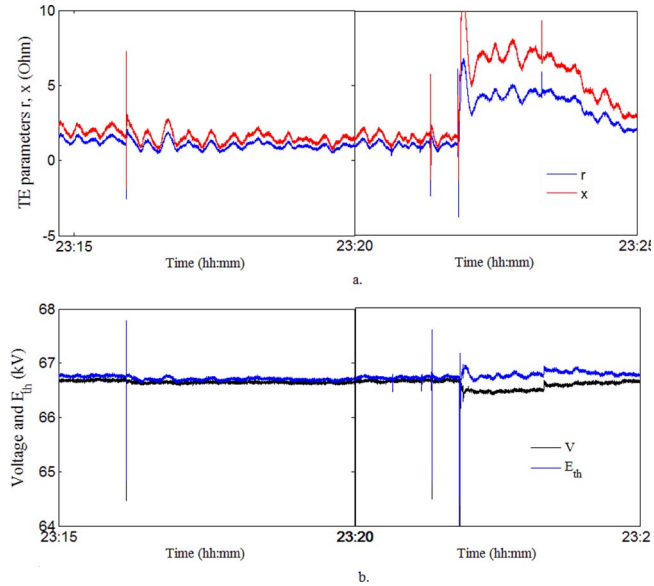

Fig. 8. TE parameters for a node in the NI network.

line. Large variations in the TE parameters taking place at approximately 23:22 are due to the tripping of the second circuit of a parallel transmission line and the commencement of a run back scheme of a generating station. At approximately 23:25, the TE parameters converge to new values higher than those at the start of the period shown on the graph due to the additional circuit tripping.

It is worthy of mention that the diagnosis of these events has been communicated to the system operator and found to be in complete agreement with their records. Also, the estimated values of the TE parameters were found to be in good agreement with the values determined from the short circuit level data at the nearby substation.

C. Bad Measurements Detection

Detecting bad data is based on the ability to trace back each of the 45 impedance values determined at each computation step. Let the set of measurement points used at a calculation step be $\mathrm{M} = \{\mathrm{m}_1, \mathrm{m}_2, \mathrm{m}_3, \mathrm{m}_4, \mathrm{m}_5\}$. As explained above, each three measurements define a straight-line impedance locus. The subsets of measurement points constituting the ten impedance loci can be formed as follows.

$\mathrm{L}_1 = \{\mathrm{m}_1, \mathrm{m}_2, \mathrm{m}_3\}$, $\mathrm{L}_2 = \{\mathrm{m}_1, \mathrm{m}_2, \mathrm{m}_4\}$, $\mathrm{L}_3 = \{\mathrm{m}_1, \mathrm{m}_2, \mathrm{m}_5\}$, $\mathrm{L}_4 = \{\mathrm{m}_1, \mathrm{m}_3, \mathrm{m}_4\}$, $\mathrm{L}_5 = \{\mathrm{m}_1, \mathrm{m}_3, \mathrm{m}_5\}$, $\mathrm{L}_6 = \{\mathrm{m}_1, \mathrm{m}_4, \mathrm{m}_5\}$, $\mathrm{L}_7 = \{\mathrm{m}_2, \mathrm{m}_3, \mathrm{m}_4\}$, $\mathrm{L}_8 = \{\mathrm{m}_2, \mathrm{m}_3, \mathrm{m}_5\}$, $\mathrm{L}_9 = \{\mathrm{m}_2, \mathrm{m}_4, \mathrm{m}_5\}$, and $\mathrm{L}_{10} = \{\mathrm{m}_3, \mathrm{m}_4, \mathrm{m}_5\}$. It is to be mentioned that these sets are formed systematically in an ordered manner. Impedance solutions are determined by intersections and are determined in an ordered manner as follows.

$\mathrm{Z}_1(\mathrm{L}_1, \mathrm{L}_2)$, $\mathrm{Z}_2(\mathrm{L}_1, \mathrm{L}_3), \ldots\ldots$, $\mathrm{Z}_9(\mathrm{L}_1, \mathrm{L}_{10})$, $\mathrm{Z}_{10}(\mathrm{L}_2, \mathrm{L}_3)$, $\mathrm{Z}_{11}(\mathrm{L}_2, \mathrm{L}_4), \ldots$, $\mathrm{Z}_{17}(\mathrm{L}_2, \mathrm{L}_{10}), \ldots\ldots\ldots\ldots$, and $\mathrm{Z}_{45}(\mathrm{L}_9, \mathrm{L}_{10})$.

Hence, if an odd impedance value is obtained, it is straightforward to find the measurement points that led to this odd value. For example, if the first TE impedance value seems to be odd,

this means that the error is in the intersection of $(\mathrm{L}_1, \mathrm{L}_2)$, i.e., the bad measurement that caused this odd value for TE impedance is enclosed in $\{\mathrm{m}_1, \mathrm{m}_2, \mathrm{m}_3\} \cup \{\mathrm{m}_1, \mathrm{m}_2, \mathrm{m}_4\}$, i.e., an element of the set $\{\mathrm{m}_1, \mathrm{m}_2, \mathrm{m}_3, \mathrm{m}_4\}$.

One bad measurement will not affect one impedance value only; it may affect up to 39 out of the 45 impedance values. Therefore, there will be more than one odd impedance value. Tracking back the other odd TE impedance values in the same manner explained for the Z_1, the bad measurement can be defined as the intersection of the sets of possible bad measurements corresponding to each of the odd impedance values.

IV. Conclusion

A new method for online determination of Thèvenin equivalent parameters at a node in a power system using local PMU measurements is presented. Despite using measurements at different time instants, the proposed method does not require synchronizing the measurements to the same time reference. Hence, it is not affected by the phase angle drift caused by system frequency changes.

An analysis for the estimated TE parameters errors is presented to gain an insight into the effect of system side changes on the TE parameters both qualitative and quantitative to help in understanding the errors arising in real-time application.

The proposed method uses 5 consecutive measurements to determine 45 possible values for the Thèvenin equivalent impedance. The frequency distribution of these values provides helpful information about the system impedance and enables, to a good extent, the diagnosis of major system events.

Application to a standard test system, the IEEE 30 bus, has demonstrated the accuracy of the method in tracking the system impedance. Additionally, it provides an insight of how the method behaves during system side changes, which may also help in detecting and diagnosing major system events. This has been verified by application to real system measurements, where the calculated Thèvenin equivalent parameters at some nodes of the NI network have been compared to those determined using the available short circuit level data. The proposed method was also able to recognize major switching events in the NI network during severe weather conditions.

Appendix

Proof of Equation (25):

As proven in the text, three measurement points form a straight line impedance locus. For number N measurements, the possible number of impedance loci, $\mathrm{N}_{\mathrm{Line}}$, will be the number of possible 3's combinations out of N:

$$N_{Line} = \binom{N}{3} = \frac{N(N-1)(N-2)}{3!}. \tag{A1}$$

Possible solutions for Z_{TH} are defined by intersections of the impedance loci. The number of possible intersections of $\mathrm{N}_{\mathrm{Line}}$ straight lines can be determined as follows:

$$N_Z = \binom{N_{Line}}{2} = \frac{N_{Line}(N_{Line}-1)}{2!}. \tag{A2}$$

Substituting for N_{Line} from (A1) into (A2)

$$\begin{aligned} N_Z &= \frac{\frac{N(N-1)(N-2)}{s!}\left(\frac{N(N-1)(N-2)}{s!}-1\right)}{2!} \\ &= \frac{N(N-1)(N-2)(N(N-1)(N-2)-3!)}{3!3!2!}. \end{aligned} \tag{A3}$$

Recalling that $3! = 6$ and $2! = 2$, it can be noticed that (A3) is the same as (25).

References

[1] J. S. Lacroix, I. Kocar, and M. Belletête, "Accelerated computation of multiphase short circuit summary for unbalanced distribution systems using the concept of selected inversion," *IEEE Trans. Power Syst.*, vol. 28, no. 2, pp. 1515–1522, May 2013.

[2] M. Dilek, R. Broadwater, and R. Sequin, "Calculating short-circuit currents in distribution systems via numerically computed Thevenin equivalents," in *Proc. IEEE PES Transmission and Distribution Conf. Expo.*, 2000, vol. 3, pp. 984–990.

[3] R. K. Gajbhiye, B. Gopi, P. Kulkarni, and S. Soman, "Computationally efficient methodology for analysis of faulted power systems with series-compensated transmission lines: A phase coordinate approach," *IEEE Trans. Power Del.*, vol. 23, no. 2, pp. 873–880, Apr. 2008.

[4] A. H. Almohammed and M. A. Abido, "An adaptive fault location algorithm for power system networks based on synchrophasor measurements," *Electr. Power Syst. Res.*, vol. 108, pp. 153–163, Mar. 2014.

[5] A. H. Almohammed and M. A. Abido, "A fully adaptive PMU-based fault location algorithm for series-compensated lines," *IEEE Trans. Power Syst.*, to be published.

[6] L. He and C. C. Liu, "Parameter identification with PMUs for instability detection in power systems with HVDC integrated offshore wind energy," *IEEE Trans. Power Syst.*, vol. 29, no. 2, pp. 775–784, Mar. 2014.

[7] J.-H. Hong and J.-K. Park, "A time-domain approach to transmission network equivalents via prony analysis for electromagnetic transients analysis," *IEEE Trans. Power Syst.*, vol. 10, no. 4, pp. 1789–1797, Nov. 1995.

[8] C. Chen, X. Liu, D. Koval, W. Xu, and T. Tayjasanant, "Critical impedance method-a new detecting harmonic sources method in distribution systems," *IEEE Trans. Power Del.*, vol. 19, no. 1, pp. 288–297, Jan. 2004.

[9] S. Abdelkader, M. H. Abdel-Rahman, and M. G. Osman, "A Norton equivalent model for nonlinear loads," in *Proc. Large Eng. Syst. Conf. Power Eng.*, Halifax, NS, Canada, 2001, pp. 63–67.

[10] S.-J. S. Tsai and K.-H. Wong, "Adaptive undervoltage load shedding relay design using Thevenin equivalent estimation," in *Proc. 2008 IEEE Power and Energy Soc. General Meeting*.

[11] W. Li, Y. Wang, and T. Chen, "Investigation on the Thevenin equivalent parameters for online estimation of maximum power transfer limits," *IET Gener., Transm., Distrib.*, vol. 4, no. 10, pp. 1180–1187, 2010.

[12] I. Šmon, G. Verbic, and F. Gubina, "Local voltage-stability index using Tallegen's theorem," *IEEE Trans. Power Syst.*, vol. 21, no. 3, pp. 1267–1275, Aug. 2006.

[13] W. Xu, I. R. Pordanjani, Y. Wang, and E. Vaahedi, "A network decoupling transform for phasor data based voltage stability analysis and monitoring," *IEEE Trans. Smart Grid*, vol. 3, no. 1, pp. 261–270, Mar. 2012.

[14] S. Corsi and G. N. Taranto, "A real-time voltage instability identification algorithm based on local phasor measurements," *IEEE Trans. Power Syst.*, vol. 23, no. 3, pp. 1271–1279, Aug. 2008.

[15] T. An, S. Zhou, J. Yu, and Y. Zhang, "Tracking Thevenin equivalent parameters on weak voltage load bus groups," in *Proc. Power Syst. Conf. Expo.*, 2006.

[16] H.-Y. Su, Y.-T. Chou, and C.-W. Liu, "Estimation of voltage stability," in *Proc. IEEE PES General Meeting*, 2012.

[17] J. H. Liu and C. C. Chu, "Wide-area measurement-based voltage stability indicators by modified coupled single-port models," *IEEE Trans. Power Syst.*, vol. 29, no. 2, pp. 756–764, Mar. 2014.

[18] A. M. Chebbo, M. R. Irving, and M. J. H. Sterling, "Voltage collapse proximity indicator, behaviour and implications," *IEE Proc.-C*, vol. 139, no. 3, pp. 241–252, May 1992.

[19] M. M. Elkateb, S. Abdelkader, and M. S. Kandil, "Linear indicator for voltage collapse in power systems," *IEE Proc.-Pt. C.*, vol. 144, no. 2, pp. 139–146, Mar. .

[20] S. Abdelkader and D. Flynn, "Graphical determination of network limits for wind power integration," *IET Gener., Transm., Distrib.*, vol. 3, no. 9, pp. 841–849, 2009.

[21] P. M. Hart, "Characterising the power system at a load busbar by measurement," *IEE Proc., Pt. C*, vol. 133, no. 2, pp. 87–94, Mar. 1986.

[22] S. A. Arefifar and W. Xu, "Online tracking of power system impedance parameters and field experiences," *IEEE Trans. Power Del.*, vol. 24, no. 4, pp. 1781–1788, Oct. 2009.

[23] S. Abdelkader, "Online Thevenin's equivalent using local PMU measurements," in *Proc. Int. Conf. Renewable Energies and Power Quality*, Spain, 2010, pp. 1–4.

[24] S. M. Abdelkader and D. J. Morrow, "Online tracking of Thévenin equivalent parameters using PMU measurements," *IEEE Trans. Power Syst.*, vol. 27, no. 2, pp. 975–983, May 2012.

[25] S. M. Abdelkader and D. J. Morrow, "Closure of discussion on: Online tracking of thévenin equivalent parameters using PMU measurements," *IEEE Trans. Power Syst.*, vol. 28, no. 2, pp. 1900–1901, May 2013.

[26] M. A. Pai, *Computer techniques in power system analysis*. New Delhi, India: Tata Mcgraw-Hill, 2006, pp. 228–231.

[27] SONI and EirGrid, "Ten year transmission forecast statement," 2013 [Online]. Available: http://www.soni.ltd.uk/media/documents/Operations/All-Island/Tenyeartransmssionforecaststatement2013.pdf

Sobhy M. Abdelkader (M'07–SM'13) was born in Salahat, Egypt, in 1961. He received the B.Sc., M.Sc., and Ph.D. degrees, all in electrical engineering, from Mansoura University, Mansoura, Egypt, in 1984, 1989, and 1995, respectively.

Since 1984, he has been employed by the Electrical Engineering Department at Mansoura University, where he is now a Professor. He joined Queen's University Belfast, Belfast, U.K., as a Senior Research Fellow in November 2007. His research interests include power system analysis and control, wind power integration into electrical grids, and electrical energy markets.

D John Morrow (M'99) was born in Dungannon, Northern Ireland, in 1959. He received the B.Sc. and Ph.D. degrees from Queen's University Belfast (QUB), Belfast, U.K., in 1982 and 1987, respectively.

He is now a Professor in electrical engineering at QUB, where he has been since 1987, with research and consulting interests in electric power systems, power system instrumentation, and embedded generation control and protection.

Dr. Morrow is a member of the IET and also a member of the IEEE Excitation Systems Subcommittee.